Nanoscale

PAPER

View Article Online
View Journal | View Issue

Cite this: *Nanoscale*, 2025, **17**, 26880

ZnO–$BaTiO_3$ vertically aligned nanocomposite (VAN) thin films with tailorable morphology and functionalities

Nirali A. Bhatt, [a] Jianan Shen,[a] James P. Barnard, [a] Juanjuan Lu, [a] Lizabeth Quigley, [a] Claire A. Mihalko, [a] Jeremy Gan, [a] Jialong Huang,[a] Benson Kunhung Tsai,[a] Abhijeet Choudhury,[a] Aleem Siddiqui,[b] Raktim Sarma[b,c] and Haiyan Wang *[a,d]

Received 23rd July 2025,
Accepted 7th October 2025

DOI: 10.1039/d5nr03110a

rsc.li/nanoscale

ZnO-based nanocomposites have been shown to possess unique properties that make them suitable for various electronic and optical applications. ZnO is a well-known piezoelectric material. Coupling it with another oxide with ferroelectric and piezoelectric behavior could lead to a composite thin film for sensing and data storage applications. In this study, ZnO–$BaTiO_3$ (BTO) nanocomposites in the form of vertically aligned nanocomposite (VAN) thin films were synthesized, and the impacts of pulsed laser deposition (PLD) laser frequency and substrate selection on the piezoelectric and ferroelectric properties were explored. Tuning the laser frequency changes the adatom diffusion length and therefore the VAN pillar diameters. Similarly, different substrates can vary the growth orientations and morphologies of the two phases in VANs due to different lattice structures between the two film phases and the substrate, enabling tuning of strain and properties. Overall, this study demonstrates the potential of ZnO–BTO VAN thin films for sensor applications because of their inherent piezoelectric and ferroelectric properties.

1. Introduction

Oxide-based nanocomposite thin films have attracted great research interest owing to their broad range of functionalities, integrated properties, property tailorability, and good thermal and chemical stability.[1] Among these oxide-based nanocomposites, vertically aligned nanocomposites (VANs) present a unique vertical thin film architecture made up of pillars growing in a matrix in an epitaxial thin film form. Typically, two immiscible phases, *e.g.*, oxide–oxide ones, such as $La_{0.5}Sr_{0.5}MnO_3$ (LSMO):ZnO,[2] LSMO:CeO_2,[3] $BiFeO_3$:Sm_2O_3,[4] $BaTiO_3$(BTO):Sm_2O_3 [5] and oxide-metal ones, such as $BaTiO_3$ (BTO):Au,[6] ZnO:Au,[7] and LSMO:Au,[8] are integrated for unique vertically coupled interfacial structures and multi-functionalities. Even a VAN system of oxide-nitride has been demonstrated.[9] The VAN architectures can be tuned through many factors such as material selection, strain, composition of the two phases, and deposition parameters, to name a few.[1] Moreover, they have been demonstrated to grow through a single step self-assembly growth process without the requirement for templating to achieve this microstructure. VANs grow through nucleation and growth processes with spontaneous ordering that results from the minimization of surface energy and elastic energy in the film. VANs stand out among other composite materials because of their multifunctionality, ease of growth, and property tunability.[1,10] Recently, studies on VANs have reported film growth that can be functional for uses such as spintronic devices,[11,12] magnetic tunneling junctions,[12] data storage devices,[13] memristors[14,15] and optical sensors.[7]

This variety of applications stems from the inherent anisotropy present in VANs because of their unique vertical structures and the integration of two dissimilar materials. As an example, many of the oxide-metal VANs have demonstrated very strong optical anisotropy and some are hyperbolic because of the dielectric oxide matrix and the conductive metal pillars.[16] Some metals are known to be ferromagnetic, plasmonic, and/or ductile.[17] Some oxides, on the other hand, are piezoelectric, ferroelectric, dielectric and/or semiconducting.

The versatile material selections in VANs present enormous opportunities in materials design and property tuning. In addition, the vertical interfacial coupling between the two film phases in VANs could result in enhanced physical properties such as strain coupling-enhanced ferroelectric properties as

[a]*School of Materials Engineering, Purdue University, West Lafayette, IN 47907, USA. E-mail: hwang00@purdue.edu*
[b]*Sandia National Laboratories, Albuquerque, NM 87123, USA*
[c]*Center for Integrated Nanotechnologies, Sandia National Laboratories, Albuquerque, NM 87123, USA*
[d]*School of Electrical and Computer Engineering, Purdue University, West Lafayette, IN 47907, USA*

seen in $BiFeO_3$–Sm_2O_3[18] and non-linear optical responses in TiN–Au and TaN–Au VAN systems.[19] Most of these vertical strain couplings have been demonstrated in cubic-based VANs on cubic substrates because VAN growth is usually preferred in epitaxial growth systems, *i.e.*, the film phases grow lattices and symmetries matched with the underlying substrates to achieve the ideal pillar-in-matrix form. Some of the cubic-based VAN examples includle $BaTiO_3$–Au on $SrTiO_3$ substrates[20] or hexagonal-based VANs on hexagonal substrates, such as ZnO:Au on sapphire.[21]

In this work, we aim to integrate ZnO with $BaTiO_3$(BTO) as a VAN thin film with tunable microstructures and physical properties. We propose to explore the morphology tuning, vertical strain coupling and physical property variations based on laser frequency and substrate selection in ZnO : BTO VANs as illustrated in the schematic shown in Fig. 1. ZnO is a functional oxide possessing many unique properties including piezoelectricity, pyroelectricity, and a large exciton binding energy due to its hexagonal wurtzite crystal structure and wide bandgap properties.[22] Incorporating ZnO into nanocomposite forms, such as ZnO–Au and ZnO–Ni,[23] has demonstrated strain-driven optical property tuning and magnetic property tuning, respectively. BTO is chosen as the secondary phase because of its interesting properties and applications. First, it is a well-known perovskite[24] which has the form of ABO_3 meaning it has an ionic nature.[25] It gets its ferroelectric properties from the displacement of the B ion, Ti.[26] It has a phase transition at the Curie temperature (T_c) of around 120 °C,[27] resulting in a phase change from tetragonal below T_c to cubic above T_c. Because of its non-centrosymmetric crystal structure, BTO exhibits piezoelectric and ferroelectric properties. Optically, it has low losses with a high dielectric constant. This makes it great for optical waveguides and memory devices.[28] Both $SrTiO_3$ (STO) and sapphire substrates were chosen, as STO matches the crystal structure of BTO, while sapphire matches that of ZnO. In addition, laser frequencies of 2 Hz and 10 Hz were explored on both substrates. 2 and 10 Hz are the laser frequencies commonly used in other laser frequency-dependent VAN studies.[11,29] Tuning the laser frequency has been shown to change the size of the VAN pillars since it directly impacts the diffusion time of the adatoms onto the substrate surface.[30] It is expected that as the laser frequency increases, the size of the pillars decreases. These changes could result in tailored piezoelectric, ferroelectric, and optical properties. Additionally, strain coupling between the two film phases is related to the tuning of the laser frequency. These films could show functionality for sensors and data storage due to their tailorable properties.

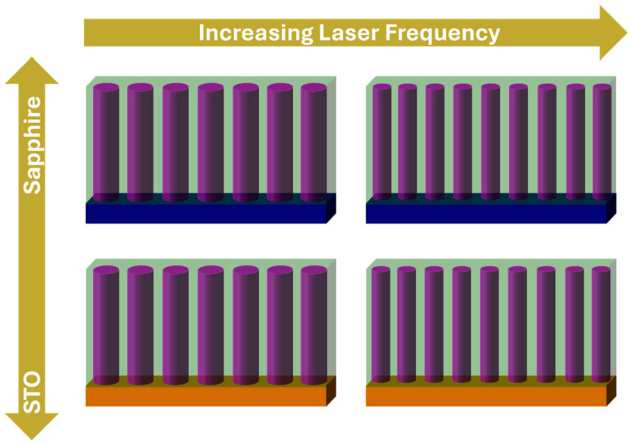

Fig. 1 Schematic of the films grown in this study. The laser frequency was tuned from 2 Hz to 10 Hz for ZnO–BTO vertically aligned nanocomposites (VANs) on both sapphire and STO substrates.

2. Results

2.1 XRD

Considering the two different phases, different deposition frequencies and two separate substrates, XRD θ–2θ scans were conducted to understand the crystallinity of these films. Fig. 2a and b show the XRD of the ZnO–BTO films grown on sapphire substrates at 10 Hz and 2 Hz, respectively. At both laser frequencies, the ZnO (0002) texture is clearly seen for the samples on the c-cut sapphire though the intensity is relatively low. This could be a result of the large amount of BTO present in the films. Regardless, there is a textured growth of ZnO. BTO, on the other hand, shows multiple peaks, thus indicating no obvious texturing. This is likely due to the differences in the crystal structure and lattice parameters from the sapphire. Unlike ZnO, which has been known to grow epitaxially on sapphire, this difference in the crystal structure and lattice parameter makes it difficult for BTO to achieve textured growth. In other words, this lack of BTO texture is a way for the BTO to accommodate the difference in the lattice parameter and strain on the sapphire substrate. Fig. S10a shows the XRD result of a reference Al-doped (AZO) as an analogue to ZnO. AZO growth shows highly textured (0001) growth on sapphire as expected.

Fig. 2c and d show the XRD of the ZnO–BTO films grown on STO substrates at 10 Hz and 2 Hz, respectively. At both laser frequencies, the BTO exhibits textured growth along (100) on the STO, which is expected due to their similar crystal structures. ZnO shows some growth as seen by the shoulder peaks of ZnO (102) and ZnO (0004) which can be seen in Fig. S2a and S2b, respectively. Similarly to the lack of textured growth of BTO on sapphire, the ZnO growth on STO demonstrates no texture due to the differences in the crystal structure and lattice parameters with STO. Fig. S10c shows the XRD of BTO on STO which looks very close to what is seen in Fig. 2c and d due to the greater concentration of BTO and its strong (00l) textured growth on the STO substrate.

In order to better understand the strain, the out of plane d-spacing was calculated and is presented in Table S1. Table S1 shows the d-spacing for the BTO(100) and ZnO(0004) peaks on the STO substrate as well as the BTO(200) and ZnO (0002) peaks on the sapphire substrate. Both 2 Hz and 10 Hz

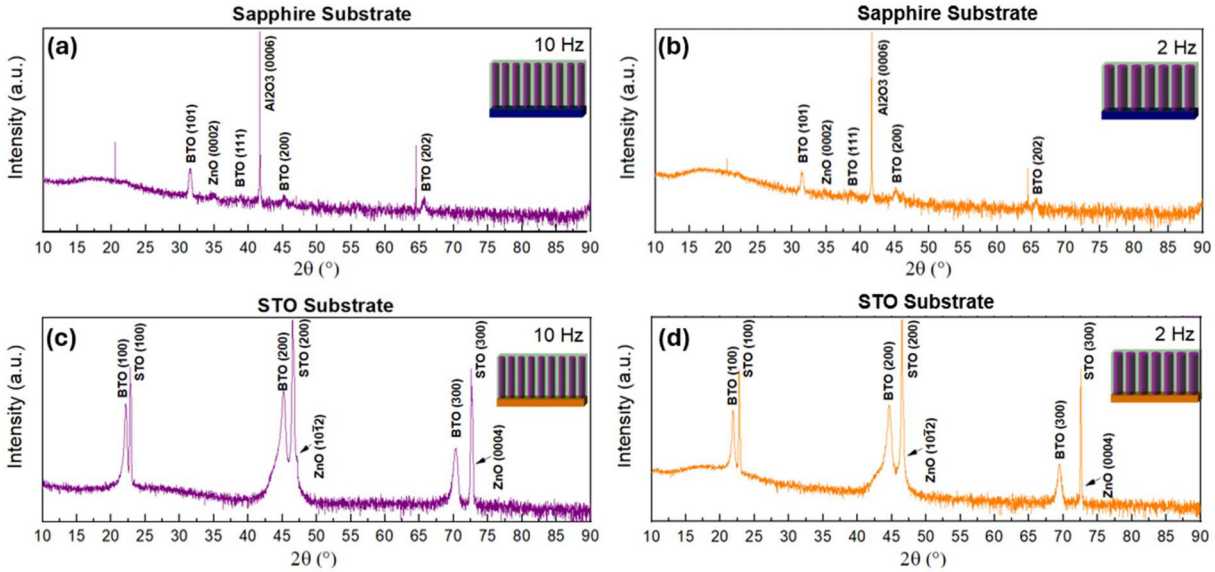

Fig. 2 XRD θ–2θ scans for the (a) 10 Hz ZnO–BTO on sapphire, (b) 2 Hz ZnO–BTO on sapphire, (c) 10 Hz ZnO–BTO on STO, and (d) 2 Hz ZnO–BTO on STO.

laser frequencies are considered. From this table, the *d*-spacing of the BTO peaks on either substrate is found to be under compression as the laser frequency increases from 2 Hz to 10 Hz. The ZnO *d*-spacing on the other hand, remains relatively stable with very little change especially for the films grown on the STO substrate. This observation is likely due to the greater concentration of BTO present in the films due to the larger molecular weight of the BTO as compared to ZnO. The choice of substrate does not seem to make a difference as both the ZnO and BTO *d*-spacings follow the same trend on both substrates. Additionally, the laser frequency for the ZnO *d*-spacing is not a factor that makes much of a difference. Overall, the high composition of BTO seems to be the cause of this behavior.

2.2 Microstructure

To explore the potential VAN architecture in these films, microstructure analysis was conducted using STEM in HAADF (high angle annular dark field) mode and EDS (energy dispersive X-ray spectroscopy). The cross-sectional images of the samples are shown in Fig. 3 and 4. First, the two frequency samples grown on c-cut sapphire are shown in Fig. 3a–h. Both demonstrate ZnO pillars grown in a BTO matrix. Interestingly, the 2 Hz sample has some ZnO pillars growing slanted and in a 'Y' shape growth, while the 10 Hz sample shows more vertical ZnO pillars. The increase in laser frequency results in an increase in pillar density which is expected as the deposition rate has a direct influence on the pillar distribution. The switch from slanted to vertical ZnO pillars can be due to a few different factors. Since the laser frequency increases, there is less resting time between each laser pulse. This causes the adatoms to have less diffusion time which could result in thinner pillars with high density. Additionally, as was seen in the XRD, the low intensity textured ZnO (0002) peaks with the multiple BTO orientations mean that the lattice mismatch between the BTO and sapphire could have resulted in these slanted pillars.

Fig. 4a–h show the two films grown on STO substrates. From the EDS mapping results, both the 2 Hz and 10 Hz films show initial vertical growth of the ZnO nanopillars for about half of the film thickness and then become slightly tilted toward the pillar top. This can also be explained by the presence of the nontextured ZnO growth as seen in the XRD for films grown on STO.

Furthermore, STEM under HAADF mode presents the contrast based on atomic number (about Z^2),[31] and it can show different grain morphologies in the films. The grains in the HAADF images in Fig. 3a and e are vertical and round at the top. In contrast, the HAADF images of the films grown on STO exhibit more rectangular grains as shown in Fig. 4a and e. This is a direct influence based on the substrate selection.

2.3 Optical properties

Considering the VAN structure, there is a likelihood that the films demonstrate unique optical behavior. Ellipsometry measurements in the wavelength range of 500 nm to 2500 nm were conducted as shown in Fig. 5. All films, regardless of laser frequency or substrate selection, demonstrate optical anisotropy as seen from the variation and differences in in-plane and out-of-plane permittivity values. Since the dielectric constant is positive, it is expected that the films will behave as oxides. The conductivity of a material greatly impacts the dielectric permittivity as well.

ZnO is typically an intrinsic n-type semiconductor due to the presence of oxygen vacancies[32] while BTO needs to be doped to achieve semiconducting behavior.[33] This means that

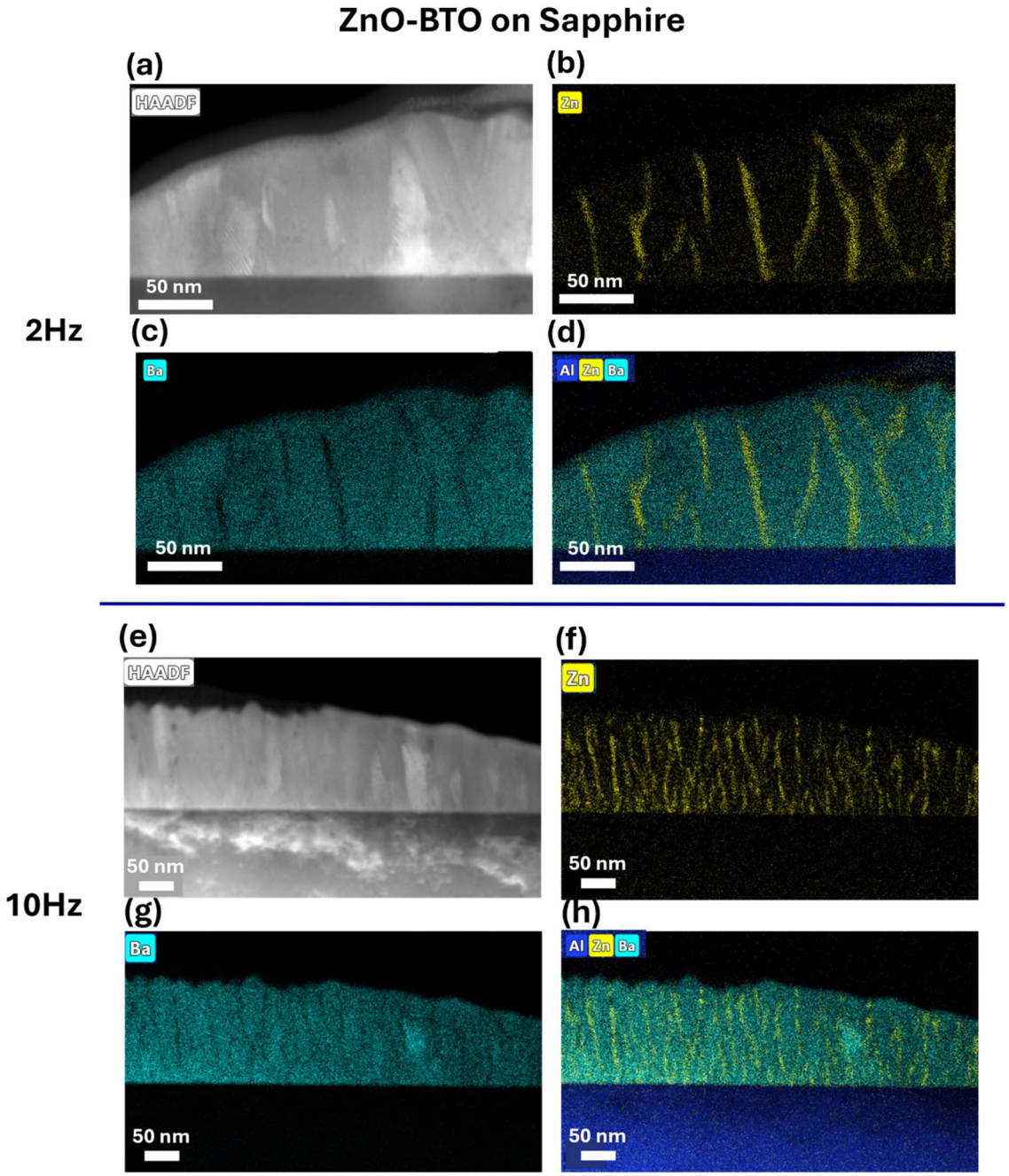

Fig. 3 Microstructure characterization of the ZnO–BTO films grown on sapphire substrates. (a) Cross-section STEM and (b) EDS mapping of Zn, (c) Ba, and (d) combined Al, Zn, and Ba for the 2 Hz film. (e) Cross-section STEM and (f) EDS mapping of Zn, (g) Ba, and (h) combined Al, Zn, and Ba for the 10 Hz film.

ZnO will present a lower permittivity, because it has more free charge carriers. BTO, on the other hand, would present a higher permittivity due to its dielectric insulating nature. This explains why the out of plane permittivity corresponding to the ZnO pillars is lower than that of the in plane which corresponds to the BTO matrix. For the reference samples shown in Fig. S10b and S10d, the results exhibit similar findings though there is no anisotropy present in the film. This highlights anisotropic optical properties as a major advantage of VAN films.

Interestingly, the in-plane permittivity is higher for all films. The sample in Fig. 5b shows the out of plane permittivity being relatively equal to the in-plane permittivity around 775 nm. A possible explanation for this could be due to a greater number of vacancies or substitutional defects.[34] These types of defects have been shown to have a higher dielectric constant at longer wavelengths.

Imaginary permittivity was also measured and can be seen in Fig. S3. All films have relatively low imaginary permittivity

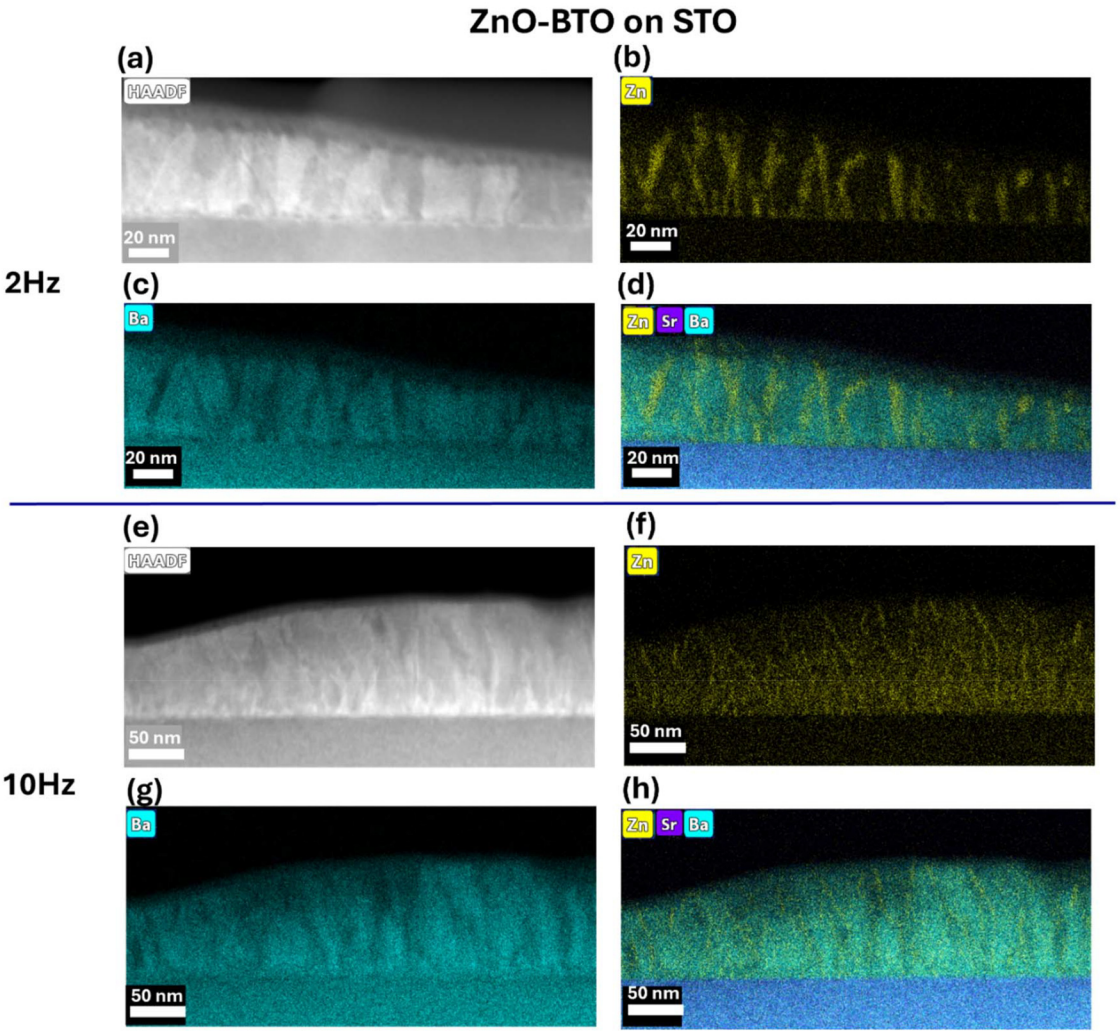

Fig. 4 Microstructure characterization of the ZnO–BTO films grown on STO substrates. (a) Cross-section STEM and (b) EDS mapping of Zn, (c) Ba, and (d) combined Sr, Zn, and Ba for the 2 Hz film. (e) Cross-section STEM and (f) EDS mapping of Zn, (g) Ba, and (h) combined Sr, Zn, and Ba for the 10 Hz film.

corresponding to low dielectric loss in the films. This makes these films suitable for photonic devices.[35]

Additionally, the refractive index (n) and extinction coefficient (k) were studied for all four films and are seen in Fig. S4. The refractive index explains the ratio between the speed of light and the speed of light in a material and explains how much the light bends. The extinction coefficient, on the other hand, describes the absorption of light in a material. For all films, the extinction coefficients of both in plane and out of plane are low, meaning that the film allows more light to pass through due to minimal absorption. Visually, this means that the films appear relatively transparent which is beneficial since transparent ceramic thin films are advantageous for use in optical applications because of their photonic quality, cost-effectiveness, and versatility.[36] Furthermore, the refractive index for the films is also relatively low, especially when compared to metals or silicon which have $n = 4$. This low refractive index would make ZnO–BTO VAN films promising for antireflective coatings.[37]

2.4 Ferroelectric and piezoelectric properties *via* PFM

One of the reasons for combining ZnO and BTO is their unique electrical properties. ZnO is piezoelectric, while BTO is piezoelectric and ferroelectric. With the growth of VAN and ZnO being the vertical pillars and BTO being the matrix, it is important to understand that the microstructure and substrate selection impact the piezoelectric and ferroelectric properties of the films. PFM (piezoresponse force microscopy) measurements were conducted. PFM gives information on the polarization of the film when a bias is applied. In this case, two types of voltages – DC voltage and AC voltage – are used to get a measurement. The scan size is changed from 5 μm to 3 μm to 8 μm, and at each size, a different/no voltage is applied. In the samples discussed next, +10 V and −10 V were applied to the

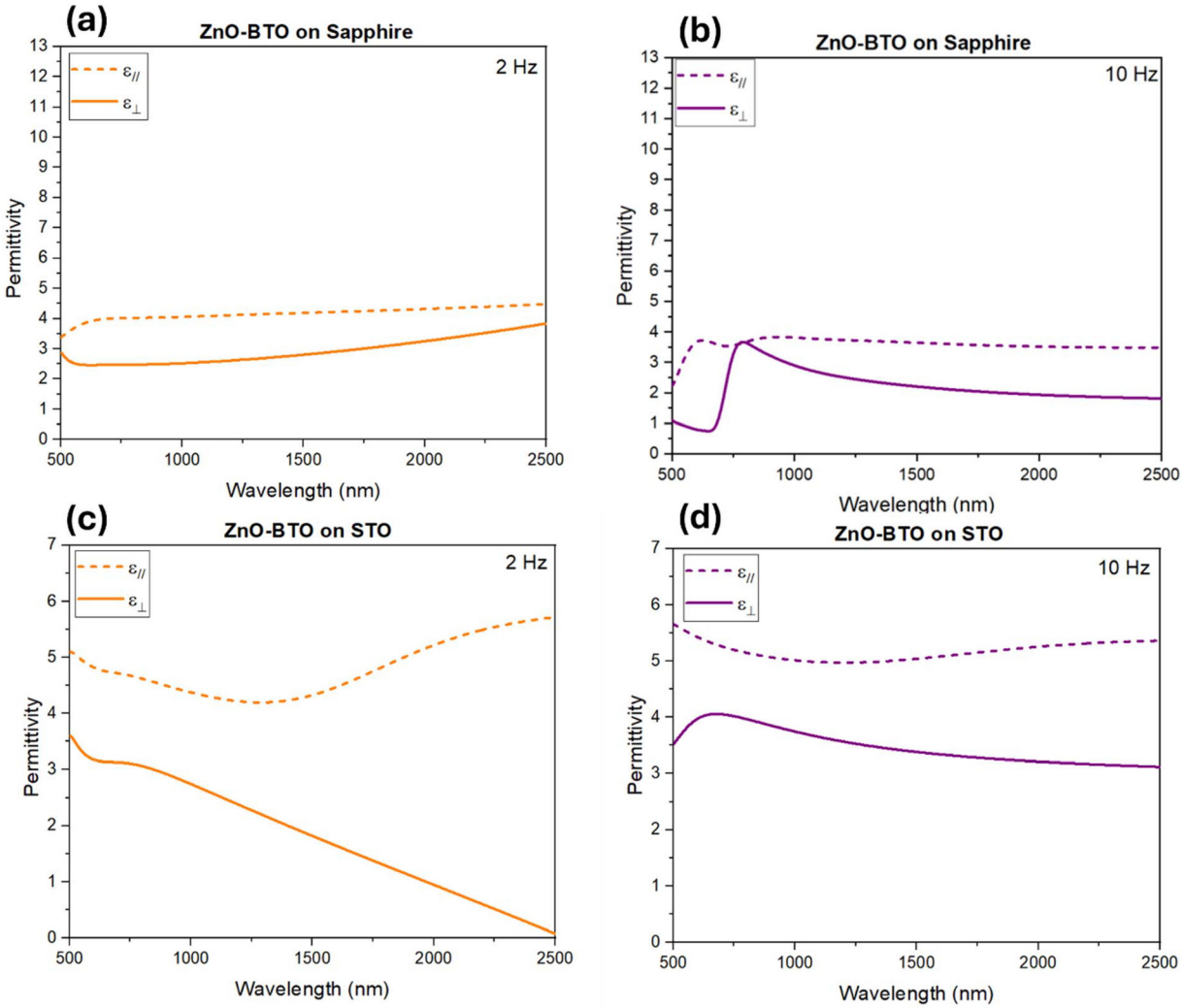

Fig. 5 Real part of the optical permittivity for the 4 films discussed. The dotted lines represent the in-plane permittivity, while the solid line is the out-of-plane permittivity for (a) 2 Hz ZnO–BTO on sapphire, (b) 10 Hz ZnO–BTO on sapphire, (c) 2 Hz ZnO–BTO on STO, and (d) 10 Hz ZnO–BTO on STO.

5 μm × 5 μm and 3 μm × 3 μm scan sizes, respectively. Then, for the 8 μm × 8 μm scan size, no bias was applied. Overall, the DC voltage 'writes' the polarization onto the sample, and the AC voltage 'reads' it[38–41] as shown in Fig. 6a, d, S5a, and S5d. If the data show a contrast in the phase map, it suggests that there are ferroelectric domains and switching behavior in the sample.

Fig. 6a shows the ferroelectric domain phase map, Fig. 6b shows the phase and amplitude, and 6c shows the d_{33} coefficient of the ZnO–BTO films grown on sapphire at 2 Hz. All d_{33} coefficient data discussed are derived from the PFM amplitude loop. In Fig. 6a, there are no ferroelectric domains as there is no obvious contrast, and the piezoelectric coefficient is about 4 pm V^{-1}. However, as the laser frequency increases to 10 Hz, there are clear ferroelectric domains (Fig. 6d) and even vertical domain switching. Fig. 6d shows the ferroelectric domain phase map, 6e shows the phase and amplitude, and 6f shows the d_{33} coefficient of the ZnO–BTO films grown on sapphire at 10 Hz. The increase in laser frequency improves the ferroelectric domains and switching behavior. Furthermore, the d_{33} coefficient also improves to about 6 pm V^{-1}. This is caused by the increased ZnO pillar density as the laser frequency increases. This results in more strained interfaces between the pillars and matrix, which can improve the piezoelectric and ferroelectric properties. Fig. S5 shows the phase map, phase and amplitude, and d_{33} coefficient of the ZnO–BTO films grown on STO substrates. Like the films grown on sapphire, the increase in laser frequency improves the contrast and thus the ferroelectric switching. However, the d_{33} coefficient decreases from about 6 pm V^{-1} to 2 pm V^{-1}. This is likely due to the lack of space between each ZnO pillar as was seen from the other three samples. *P–E* loops of some of the films were taken, and only some of the films demonstrated ferroelectric hysteresis as shown in Fig. S6a and S6b.

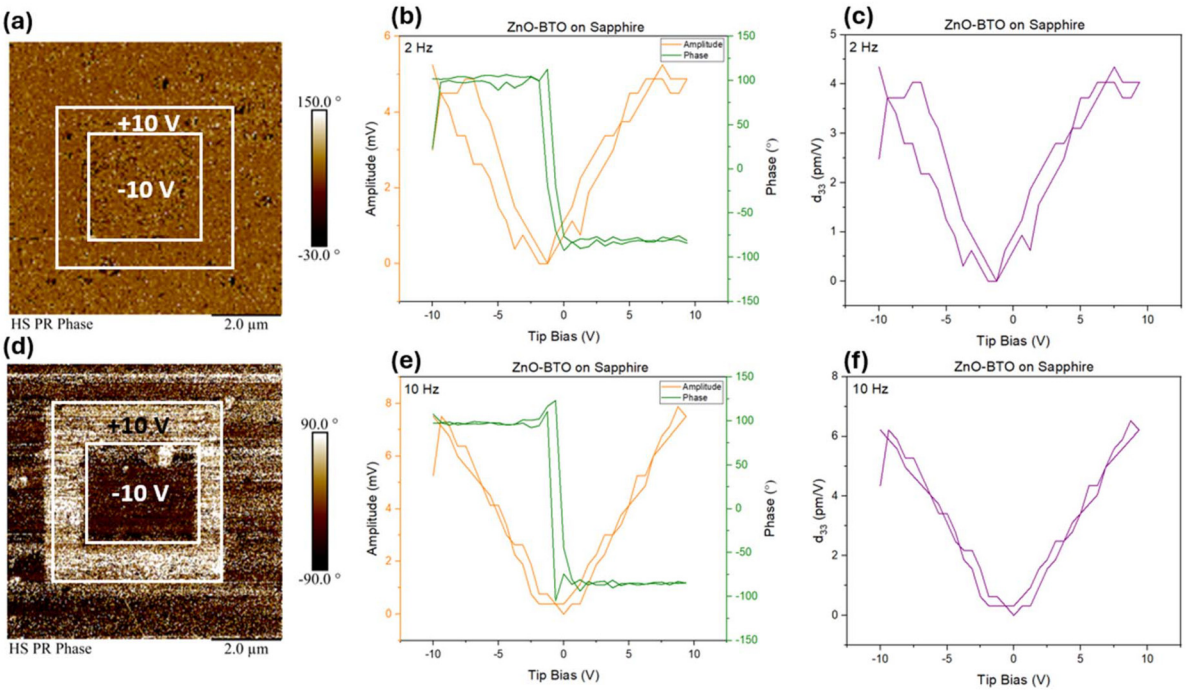

Fig. 6 (a) PFM phase map, (b) phase and amplitude, and (c) d_{33} coefficient for the 2 Hz ZnO–BTO on sapphire. (d) PFM phase map, (e) phase and amplitude, and (f) d_{33} coefficient for the 10 Hz ZnO–BTO on sapphire.

3. Discussion

This study seeks to better understand how the ZnO–BTO thin films change based on laser frequency and substrate selection. A 3 : 2 molar ratio of ZnO to BTO has been proven to be successful in growing VANs. In comparison, a 2 : 3 molar ratio of ZnO to BTO was tried as well. This concentration did not result in the growth of VANs but rather both phases were mixed forming a homogeneous thin film. An example of this homogeneous growth is shown in Fig. S7 with the TEM and EDS of the 10 Hz 2 : 3 molar ratio ZnO–BTO grown on STO. It was found that the concentration of ZnO and BTO is important. A possible mechanism for this observation could be the difference in the lattice structure between ZnO and BTO. ZnO has a wurtzite hexagonal structure with lattice constants of a = b = 3.25 Å and c = 5.2 Å.[42] BTO on the other hand has a tetragonal structure with a = 3.99 Å and c = 4.0 Å.[43] Additionally, the amount of BTO in this case is much greater in the 2 : 3 ZnO–BTO than that in the 3 : 2 ZnO–BTO, which results in a BTO-dominant nanocomposite. ZnO becomes a very minor phase in the overall nanocomposite, and thus, the film becomes homogeneous without obvious pillars observed. Other factors could be related to the relative growth rates between the two materials and the difference in surface energy between ZnO and BTO, which could all result in this BTO-dominant nanocomposite.[16]

Further investigation was conducted on the 2 : 3 (40 mol%–60 mol%) ZnO–BTO molar ratio films. First, XRD of the target was recorded as shown in Fig. S8. Compared to the target XRD of the 3 : 2 ZnO–BTO molar ratio in Fig. S1, there are understandably lower intensity peaks of the ZnO since there is less ZnO in the 2 : 3 ratio. PFM measurements were also conducted for the four samples, as can be seen in Fig. S9. The 2 : 3 ZnO–BTO grown on sapphire at both laser frequencies did not demonstrate ferroelectric domains, but the growth on STO did. This means that the growth on sapphire does not have switchable ferroelectric domains, possibly resulting from the intermixing of ZnO and BTO and their 2 distinct crystal structures. STO one shows ferroelectric switching, perhaps from a larger strain in the film.[39] It is interesting how ordered growth in the VAN shows switching for the sapphire substrate, and this is likely from the interface strain between the ZnO and BTO and more controlled growth. Fig. S6c and S6d show the *P*–*E* loops that demonstrated proper ferroelectric hysteresis. The hysteresis in the 2 : 3 ratio films is improved, perhaps due to the greater amount of BTO than that seen in the 3 : 2 ratio films. Since BTO is a ferroelectric material, it contributed to the improved hysteresis.

Furthermore, it is important to note that molar ratios need to be considered carefully when mixing a complex oxide with a simple oxide. Specifically, the higher molecular weight of BTO needs to be accounted for. For PLD targets made from powders as in this study, the larger molecular weight of BTO (233.207 g mol^{-1}) than ZnO (81.38 g mol^{-1}) can result in the addition of a greater amount of BTO powder which ultimately means there is more BTO. This is why ZnO grows as the pillars while BTO is the matrix. A deep look into composition tuning would show at what concentrations VAN growth is possible.

Other technologically important substrates, such as silicon, can be explored for VAN growth in future device integration.

The ZnO–BTO material system is a new oxide–oxide VAN system with very few prior studies showing VAN type growth. One study demonstrating ZnO–BTO VAN was by Wang *et al.*[44] where the memristive properties of ZnO–BTO were investigated. Misra *et al.*[45] grew Au–ZnO–BTO VAN on an STO substrate as a demonstration of three phase VAN growth using a BTO–Au seed structure. They also reported the tilting of ZnO pillars after thickness reaching the range of 35–40 nm. It was also predicted that this tilting results from the minimization of strain energy which accounts for the increase in surface free energy. Additionally, they reported ferroelectric switching and a d_{33} coefficient near 10 pm V^{-1} which is close to what was reported for the sample in Fig. 6f above. Clearly, there are few reports of ZnO–BTO VAN, but the material system is very promising because of the combination of oxides, their out of plane strain component, and anisotropy. Future work can aim to understand the role of other deposition parameters, the addition of different dopants, and even phases to comprehend how desired properties can be achieved. Furthermore, the growth of epitaxial ZnO–BTO on Si can be promising as shown by Tiwari *et al.*[46] with the epitaxial growth of ZnO on Si(111). Prior studies of other oxides prove that this can be possible. For example, both epitaxial BTO–CeO_2 VAN[47] and $La_{0.7}Sr_{0.3}MnO_3$:NiO VAN[48] on Si (001) were achieved with multiple buffer layers and showed a ferroelectric response and an exchange bias effect, respectively. There are challenges to achieving direct epitaxial growth on Si as seen by the incorporation of buffer layers to accommodate the difference in lattice mismatch. In addition, oxidation of Si substrates is possible as well, and the various Si orientations add to the challenges of achieving desired growth. While challenges exist for epitaxial growth on Si, investigation of proper growth parameters could allow for desired growth.

Furthermore, the scalability of the PLD-based VAN is an important consideration especially if the growth of this ZnO–BTO VAN is to be used in industrial applications. In recent years, PLD has been shown to be scalable through the use of a slit system to overcome plume broadening[49] and a laser-scanning method to address uniformity of the film thickness over the wafer scale.[50] Additional motorized substrate handling and the roll–roll process method have been developed to coat uniform films on substrates up to 12 inches in diameter[51] and meter-long tapes for high-temperature superconductor coated conductors.[52] Overall, achieving scaled-up VAN growth with PLD requires the ability to grow thick enough films that are uniform while maintaining target stoichiometry. To achieve this, it is crucial to ensure that the large substrate is heated evenly so that diffusion processes can occur and the lasers ablating the target create a plume large enough to grow a uniform film.

The various properties present in the ZnO–BTO material system, and the tuning seen depending on the substrate and laser frequency, make it promising for multiple applications. First, BTO is a great ferroelectric material alternative for the well-known lead zirconate titanate (PZT), considering its lead-free oxide, low fabrication cost, and good ferroelectric and piezoelectric properties.[53,54] Additionally, the low dielectric loss of BTO makes these ZnO–BTO VANs useful in dynamic random access memory devices, capacitors, and optical waveguides.[28] Additionally, the VAN architecture allows for thicker strained films if needed due to the out of plane strain coupling. Therefore, the ferroelectric properties of the VAN films are not limited by the strained single phase thin films under the critical thickness.[55] Though further investigation is needed to use the ZnO–BTO VANs in practical applications, the data presented in this work suggests that the ZnO–BTO VANs could be a unique choice for thick ferroelectric thin films and a good material system for ferroelectric and piezoelectric applications.

4. Conclusion

This work explores the VAN morphology and property tuning in ZnO–BTO with the ZnO–BTO molar ratio of 3 : 2. The crystallinity of the films varied depending on the substrates. The films grown on sapphire demonstrated epitaxial and/or textured growth of ZnO, while those grown on STO showed epitaxial and/or textured growth of BTO. The well-suited crystal structure of sapphire to ZnO and STO to BTO aided in this growth. Microstructurally, the ZnO grew as VAN pillars, while BTO was the matrix. On both substrates, as the laser frequency increases, the size of the ZnO pillars decreases as expected. Optically, the films were all anisotropic, with optical permittivity that shows low losses, a property known to BTO. The extinction coefficient was low for all four films, meaning that less light is absorbed, suggesting optically transparent films. Ferroelectric and piezoelectric properties were determined, and ferroelectric switching was observed as well as tuning of the d_{33} coefficient. This work presents a ZnO-based VAN material system that demonstrates laser frequency tuning of piezoelectric and ferroelectric properties for future sensing and optical applications.

5. Experimental

5.1 Thin film growth

Pulsed laser deposition (PLD) was the thin film growth method used to grow the ZnO–BTO VAN films onto sapphire (0001) and STO (001) substrates. A 3 : 2 molar ratio (60 mol%–40 mol%) ZnO–BTO nanocomposite target was made by mixing ZnO and $BaTiO_3$ powders, pressing the mixture, and sintering at 950 °C for 6 hours. Al-doped ZnO (AZO) was used as the conductive bottom electrode for electrical measurements on sapphire and was grown below the ZnO–BTO. The AZO was made by mixing and sintering ZnO and Al_2O_3 powders with 2 weight percent Al_2O_3 for a 6-gram target. The AZO target was sintered at 1100 °C for 11 hours. During the AZO deposition, 1250 pulses at 780 °C, 5 Hz, and 150 mTorr

oxygen background were used. Then the AZO film was cooled to 500 °C and annealed for 30 minutes with 100 Torr oxygen background pressure. Strontium ruthenate ($SrRuO_3$, SRO) was used as the conductive bottom electrode for electrical measurements on STO and was grown underneath the ZnO–BTO. During SRO deposition, 3000 pulses at 750 °C, 5 Hz, with 40 mTorr oxygen background pressure were applied. Then, it was cooled in a 40 mTorr background. The ZnO–BTO was grown on sapphire (with or without the AZO) using ~4900 pulses, at 780 °C, 100 mTorr oxygen background pressure. Then the film was cooled to 500 °C and annealed for 30 minutes with 100 Torr oxygen background pressure. The laser frequency was varied to either 2 Hz or 10 Hz. The ZnO–BTO was grown on STO (with or without the SRO) using 3000 pulses at 780 °C with a 100 mTorr oxygen background pressure. Then it was cooled in a 100 Torr oxygen background. The laser frequency was varied to either 2 Hz or 10 Hz. For all growths, a laser energy of 450 mJ was used.

5.2 Microstructure characterization

The microstructure characterization was conducted using X-ray diffraction (XRD) with ±0.1 nm error values for the *d*-spacing, transmission electron microscopy (TEM), scanning transmission electron microscopy (STEM), and energy-dispersive X-ray spectroscopy (EDS). A Malvern PANalytical Empyrean X-ray diffractometer (XRD) from Worcestershire, UK, was used to conduct θ–2θ scans with Cu K_α radiation (λ = 0.154 nm). The cross-section of TEM samples was made using a standard sample preparation procedure consisting of manual grinding, dimple polishing, and ion milling (PIPS 695 system, 5 keV).

5.3 Optical characterization

Optical measurements were performed using a J.A. Woollam RC2 spectroscopic ellipsometer for ellipsometry measurements. A B-spline model coupled with a uniaxial model was applied to perform optical permittivity measurements in the range of 250–2500 nm. All samples had a mean square error (MSE) below 5. Specifically, Fig. 5a with MSE = 3.2, Fig. 5b with MSE = 3.7, Fig. 5c with MSE = 3.9, and Fig. 5d with MSE = 2.8.

5.4 Electrical characterization

Piezoelectric force microscopy (PFM) measurements were conducted with a Bruker Dimension Icon that used SCM-PIT probes. This includes the PFM phase map as well as the d_{33} coefficient measurement. The d_{33} coefficient was calculated using the PFM amplitude loop.

The ferroelectric hysteresis (*P*–*E*) loop measurement was conducted using a Radiant Technologies Precision LC II ferroelectric tool.

Author contributions

Conceptualization, investigation, methodology, writing – original draft, and writing – review and editing, N. A. B.; investigation and writing – review and editing, J. S., J. P. B., J. L., L. Q., C. A. M., J. G., J. H., and B. K. T.; investigation, A. C.; funding acquisition, supervision, and writing – review and editing, R. S. and A. S.; conceptualization, funding acquisition, supervision, and writing – review and editing, H. W.

Conflicts of interest

The authors declare no conflicts of interest. The funders had no role in the design of the study, in the collection, analyses, or interpretation of data, in the writing of the manuscript, or in the decision to publish the results.

Data availability

The data supporting this article have been included as part of the supplementary information (SI). Supplementary information is available. See DOI: https://doi.org/10.1039/d5nr03110a.

Acknowledgements

This work is funded by the U.S. Department of Energy, Office of Science, Basic Energy Sciences with award no. DE-SC0020077. N. A. B. thanks the support from the Purdue University Andrews Graduate Fellowship. N. A. B. and L. Q. acknowledge the support from the Sandia Diversity Fellowship Program at Sandia National Laboratories. This work was performed in part at the Center for Integrated Nanotechnologies, an Office of Science User Facility operated by the U.S. Department of Energy (DOE) Office of Science. Part of this work was performed under the Laboratory Directed Research and Development (LDRD) program at Sandia National Laboratories. Sandia National Laboratories is a multimission laboratory managed and operated by National Technology & Engineering Solutions of Sandia, LLC, a wholly owned subsidiary of Honeywell International Inc., for the U.S. Department of Energy's National Nuclear Security Administration under contract DE-NA0003525. This paper describes objective technical results and analysis. Any subjective views or opinions that might be expressed in the paper do not necessarily represent the views of the U.S. Department of Energy or the United States Government.

References

1 X. Sun, J. L. MacManus-Driscoll and H. Wang, Spontaneous Ordering of Oxide-Oxide Epitaxial Vertically Aligned Nanocomposite Thin Films, *Annu. Rev. Mater. Res.*, 2020, **50**, 229–253, DOI: 10.1146/annurev-matsci-091719-112806.

2 A. Chen, Z. Bi, C.-F. Tsai, J. Lee, Q. Su, X. Zhang, Q. Jia, J. L. MacManus-Driscoll and H. Wang, Tunable Low-Field

Magnetoresistance in (La0.7Sr0.3MnO3)0.5:(ZnO)0.5 Self-Assembled Vertically Aligned Nanocomposite Thin Films, *Adv. Funct. Mater.*, 2011, **21**, 2423–2429, DOI: 10.1002/adfm.201002746.

3 A. Chen, Z. Bi, H. Hazariwala, X. Zhang, Q. Su, L. Chen, Q. Jia, J. L. MacManus-Driscoll and H. Wang, Microstructure, Magnetic, and Low-Field Magnetotransport Properties of Self-Assembled (La0.7Sr0.3MnO3)0.5:(CeO_2)0.5 Vertically Aligned Nanocomposite Thin Films, *Nanotechnology*, 2011, **22**, 315712, DOI: 10.1088/0957-4484/22/31/315712.

4 J. L. MacManus-Driscoll, P. Zerrer, H. Wang, H. Yang, J. Yoon, A. Fouchet, R. Yu, M. G. Blamire and Q. Jia, Strain Control and Spontaneous Phase Ordering in Vertical Nanocomposite Heteroepitaxial Thin Films, *Nat. Mater.*, 2008, **7**, 314–320, DOI: 10.1038/nmat2124.

5 W. Zhang, A. Chen, Z. Bi, Q. Jia, J. L. MacManus-Driscoll and H. Wang, Interfacial Coupling in Heteroepitaxial Vertically Aligned Nanocomposite Thin Films: From Lateral to Vertical Control, *Curr. Opin. Solid State Mater. Sci.*, 2014, **18**, 6–18, DOI: 10.1016/j.cossms.2013.07.007.

6 D. Zhang, S. Misra, L. Li, X. Wang, J. Jian, P. Lu, X. Gao, X. Sun, Z. Qi, M. Kalaswad, *et al.*, Tunable Optical Properties in Self-Assembled Oxide-Metal Hybrid Thin Films via Au-Phase Geometry Control: From Nanopillars to Nanodisks, *Adv. Opt. Mater.*, 2020, **8**, 1901359, DOI: 10.1002/adom.201901359.

7 N. A. Bhatt, R. L. Paldi, J. P. Barnard, J. Lu, Z. He, B. Yang, C. Shen, J. Song, R. Sarma, A. Siddiqui, *et al.*, ZnO-Au Hybrid Metamaterial Thin Films with Tunable Optical Properties, *Crystals*, 2024, **14**, 65, DOI: 10.3390/cryst14010065.

8 J. Lu, R. L. Paldi, Y. Pachaury, D. Zhang, H. Wang, M. Kalaswad, X. Sun, J. Liu, X. L. Phuah, X. Zhang, *et al.*, Ordered Hybrid Metamaterial of La0.7Sr0.3MnO3–Au Vertically Aligned Nanocomposites Achieved on Templated SrTiO3 Substrate, *Mater. Today Nano*, 2021, **15**, 100121, DOI: 10.1016/j.mtnano.2021.100121.

9 X. Wang, H. Wang, J. Jian, B. X. Rutherford, X. Gao, X. Xu, X. Zhang and H. Wang, Metal-Free Oxide-Nitride Heterostructure as a Tunable Hyperbolic Metamaterial Platform, *Nano Lett.*, 2020, **20**, 6614–6622, DOI: 10.1021/acs.nanolett.0c02440.

10 S. Misra and H. Wang, Review on the Growth, Properties and Applications of Self-Assembled Oxide–Metal Vertically Aligned Nanocomposite Thin Films—Current and Future Perspectives, *Mater. Horiz.*, 2021, **8**, 869–884, DOI: 10.1039/D0MH01111H.

11 L. Quigley, J. Shen, J. Lu, C. A. Mihalko, J. P. Barnard, Y. Zhang, N. A. Bhatt, K. Evancho, R. Sarma, A. Siddiqui, *et al.*, Target Configuration Effect on Microstructures and Properties of Vertically Aligned Nanocomposites, *Cryst. Growth Des.*, 2024, **24**, 8929–8936, DOI: 10.1021/acs.cgd.4c00958.

12 Y. Zhang, J. Song, P. Lu, J. Deitz, D. Zhang, H. Dou, J. Shen, Z. Hu, X. Zhang and H. Wang, Tunable Magnetic and Optical Anisotropy in ZrO_2 –Co Vertically Aligned Nanocomposites, *Adv. Mater. Interfaces*, 2023, **10**, 2300150, DOI: 10.1002/admi.202300150.

13 J. Huang, L. Li, Z. Hu, B. K. Tsai, J. Huang, J. Shen, Y. Zhang, J. P. Barnard, J. Song and H. Wang, Ultrathin Ternary FeCoNi Alloy Nanoarrays in $BaTiO_3$ Matrix for Room-Temperature Multiferroic and Hyperbolic Metamaterial, *Nano Lett.*, 2024, **24**, 10081–10089, DOI: 10.1021/acs.nanolett.4c02036.

14 Z. Hu, H. Dou, Y. Zhang, J. Shen, L. Ahmad, S. Han, E. G. Hollander, J. Lu, Y. Zhang, Z. Shang, *et al.*, Integration of CeO_2-Based Memristor with Vertically Aligned Nanocomposite Thin Film: Enabling Selective Conductive Filament Formation for High-Performance Electronic Synapses, *ACS Appl. Mater. Interfaces*, 2024, **16**, 64951–64962, DOI: 10.1021/acsami.4c10687.

15 H. Dou, Z. Lin, Z. Hu, B. K. Tsai, D. Zheng, J. Song, J. Lu, X. Zhang, Q. Jia, J. L. MacManus-Driscoll, *et al.*, Self-Assembled Au Nanoelectrodes: Enabling Low-Threshold-Voltage HfO2-Based Artificial Neurons, *Nano Lett.*, 2023, **23**, 9711–9718, DOI: 10.1021/acs.nanolett.3c02217.

16 J. Song and H. Wang, A Material Design Guideline for Self-Assembled Vertically Aligned Nanocomposite Thin Films, *J. Phys. Mater.*, 2025, **8**, 012002, DOI: 10.1088/2515-7639/ad9bee.

17 M. J. Cordill, P. Kreiml and C. Mitterer, Materials Engineering for Flexible Metallic Thin Film Applications, *Materials*, 2022, **15**, 926, DOI: 10.3390/ma15030926.

18 A. Fouchet, H. Wang, H. Yang, J. Yoon, Q. Jia and J. L. Macmanus-driscoll, Spontaneous Ordering, Strain Control, and, Multifunctionality in Vertical Nanocomposite Heteroepitaxial Films, *IEEE Trans. Ultrason., Ferroelectr., Freq. Control*, 2009, **56**, 1534–1538, DOI: 10.1109/TUFFC.2009.1217.

19 J. Huang, X. Wang, N. L. Hogan, S. Wu, P. Lu, Z. Fan, Y. Dai, B. Zeng, R. Starko-Bowes, J. Jian, *et al.*, Nanoscale Artificial Plasmonic Lattice in Self-Assembled Vertically Aligned Nitride–Metal Hybrid Metamaterials, *Adv. Sci.*, 2018, **5**, 1800416, DOI: 10.1002/advs.201800416.

20 X. Wang and H. Wang, *Recent Advances in Vertically Aligned Nanocomposites with Tunable Optical Anisotropy: Fundamentals and Beyond*. 2021.

21 N. A. Bhatt, R. L. Paldi, J. P. Barnard, J. Lu, Z. He, B. Yang, C. Shen, J. Song, R. Sarma, A. Siddiqui, *et al.*, ZnO-Au Hybrid Metamaterial Thin Films with Tunable Optical Properties, *Crystals*, 2024, **14**, 65, DOI: 10.3390/cryst14010065.

22 D. K. Sharma, S. Shukla, K. K. Sharma and V. Kumar, A Review on ZnO: Fundamental Properties and Applications, *Mater. Today: Proc.*, 2022, **49**, 3028–3035, DOI: 10.1016/j.matpr.2020.10.238.

23 Morphology and Property Tuning in ZnO–Ni Hybrid Metamaterials in Vertically Aligned Nanocomposite (VAN) Form - Nanoscale Advances (RSC Publishing) Available online: https://pubs.rsc.org/en/content/articlelanding/2025/na/d5na00207a (accessed on 28 May 2025).

24 B. Ertuğ, The Overview of The Electrical Properties of Barium Titanate, *Am. J. Eng. Res.*, 2013, **02**, 01–07.
25 A. Bussmann-Holder, K. Roleder and J.-H. Ko, What Makes the Difference in Perovskite Titanates?, *J. Phys. Chem. Solids*, 2018, **117**, 148–157, DOI: 10.1016/j.jpcs.2018.02.025.
26 L. B. Kong, S. Li, T. S. Zhang, J. W. Zhai, F. Y. C. Boey and J. Ma, Electrically Tunable Dielectric Materials and Strategies to Improve Their Performances, *Prog. Mater. Sci.*, 2010, **55**, 840–893, DOI: 10.1016/j.pmatsci.2010.04.004.
27 Z. Chlup, D. Drdlík, H. Hadraba, O. Ševeček, F. Šiška, J. Erhart and K. Maca, Temperature Effect on Elastic and Fracture Behaviour of Lead-Free Piezoceramic BaTiO3, *J. Eur. Ceram. Soc.*, 2023, **43**, 1509–1522, DOI: 10.1016/j.jeurceramsoc.2022.11.030.
28 K. Tewatia, A. Sharma, M. Sharma and A. Kumar, Factors Affecting Morphological and Electrical Properties of Barium Titanate: A Brief Review, *Mater. Today: Proc.*, 2021, **44**, 4548–4556, DOI: 10.1016/j.matpr.2020.10.813.
29 X. Gao, D. Zhang, X. Wang, J. Jian, Z. He, H. Dou and H. Wang, Vertically Aligned Nanocomposite (BaTiO 3) 0.8 : (La 0.7 Sr 0.3 MnO 3) 0.2 Thin Films with Anisotropic Multifunctionalities, *Nanoscale Adv.*, 2020, **2**, 3276–3283, DOI: 10.1039/D0NA00232A.
30 N. A. Shepelin, Z. P. Tehrani, N. Ohannessian, C. W. Schneider, D. Pergolesi and T. Lippert, A Practical Guide to Pulsed Laser Deposition, *Chem. Soc. Rev.*, 2023, **52**, 2294–2321, DOI: 10.1039/D2CS00938B.
31 Z. Wang, M. Saito, K. P. McKenna, L. Gu, S. Tsukimoto, A. L. Shluger and Y. Ikuhara, Atom-Resolved Imaging of Ordered Defect Superstructures at Individual Grain Boundaries, *Nature*, 2011, **479**, 380–383, DOI: 10.1038/nature10593.
32 L. Liu, Z. Mei, A. Tang, A. Azarov, A. Kuznetsov, Q.-K. Xue and X. Du, Oxygen Vacancies: The Origin of n-Type Conductivity in ZnO, *Phys. Rev. B*, 2016, **93**, 235305, DOI: 10.1103/PhysRevB.93.235305.
33 M. Maraj, A. Fatima, S. S. Ali, U. Hira, M. Rizwan, Z. Usman, W. Sun and A. Shaukat, Taming the Optical Response via (Ca:Zr) Co-Doped Impurity in c-BaTiO3: A Comprehensive Computational Insight, *Mater. Sci. Semicond. Process.*, 2022, **144**, 106573, DOI: 10.1016/j.mssp.2022.106573.
34 D. Kaur, A. Bharti, T. Sharma and C. Madhu, Dielectric Properties of ZnO-Based Nanocomposites and Their Potential Applications, *Int. J. Opt.*, 2021, **2021**, 9950202, DOI: 10.1155/2021/9950202.
35 D. Urbonas, R. F. Mahrt and T. Stöferle, Low-Loss Optical Waveguides Made with a High-Loss Material, *Light:Sci. Appl.*, 2021, **10**, 15, DOI: 10.1038/s41377-020-00454-w.
36 O. J. Akinribide, G. N. Mekgwe, S. O. Akinwamide, F. Gamaoun, C. Abeykoon, O. T. Johnson and P. A. Olubambi, A Review on Optical Properties and Application of Transparent Ceramics, *J. Mater. Res. Technol.*, 2022, **21**, 712–738, DOI: 10.1016/j.jmrt.2022.09.027.
37 C. Harendt and H.-G. Graf, 3.08 - Micro-Imaging Systems, in *Comprehensive Microsystems*, ed. Y. B. Gianchandani, O. Tabata and H. Zappe, Elsevier, Oxford, 2008, pp. 267–291. ISBN 978-0-444-52190-3.
38 J. P. Barnard, J. Shen, Y. Zhang, J. Lu, J. Song, A. Siddiqui, R. Sarma and H. Wang, Improved Epitaxial Growth and Multiferroic Properties of $Bi_3Fe_2Mn_2O_x$ Using CeO_2 Re-Seeding Layers, *Nanoscale Adv.*, 2023, **5**, 5850–5858, DOI: 10.1039/D3NA00512G.
39 J. P. Barnard, R. L. Paldi, M. Kalaswad, Z. He, H. Dou, Y. Zhang, J. Shen, D. Zheng, N. R. Dilley, R. Sarma, *et al.*, Epitaxial Growth of Aurivillius Bi3Fe2Mn2Ox Supercell Thin Films on Silicon, *Cryst. Growth Des.*, 2023, **23**, 2248–2256, DOI: 10.1021/acs.cgd.2c01300.
40 J. Shen, Z. He, D. Zhang, P. Lu, J. Deitz, Z. Shang, M. Kalaswad, H. Wang, X. Xu and H. Wang, Tunable Physical Properties in Bi-Based Layered Supercell Multiferroics Embedded with Au Nanoparticles, *Nanoscale Adv.*, 2022, **4**, 3054–3064, DOI: 10.1039/D2NA00169A.
41 How Does Piezo Response Force Microscopy Work? Available online: https://www.azonano.com/article.aspx?ArticleID=6333 (accessed on 22 March 2025).
42 C. F. Klingshirn, B. K. Meyer, A. Waag, A. Hoffmann and J. Geurts, *Zinc Oxide: From Fundamental Properties Towards Novel Applications*, Springer Series in Materials Science, Springer Berlin Heidelberg, Berlin, Heidelberg, 2010, Vol. 120; ISBN: 978-3-642-10576-0.
43 L. Mazet, S. M. Yang, S. V. Kalinin, S. Schamm-Chardon and C. Dubourdieu, A Review of Molecular Beam Epitaxy of Ferroelectric BaTiO3 Films on Si, Ge and GaAs Substrates and Their Applications, *Sci. Technol. Adv. Mater.*, 2015, **16**, 036005, DOI: 10.1088/1468-6996/16/3/036005.
44 G. Wang, F. Sun, S. Zhou, Y. Zhang, F. Zhang, H. Wang, J. Huang and Y. Zheng, Enhanced Memristive Performance via a Vertically Heterointerface in Nanocomposite Thin Films for Artificial Synapses, *ACS Appl. Mater. Interfaces*, 2024, **16**, 12073–12084, DOI: 10.1021/acsami.3c18146.
45 S. Misra, L. Li, D. Zhang, J. Jian, Z. Qi, M. Fan, H.-T. Chen, X. Zhang and H. Wang, Self-Assembled Ordered Three-Phase Au–BaTiO3–ZnO Vertically Aligned Nanocomposites Achieved by a Templating Method, *Adv. Mater.*, 2019, **31**, 1806529, DOI: 10.1002/adma.201806529.
46 A. Tiwari, M. Park, C. Jin, H. Wang, D. Kumar and J. Narayan, Epitaxial Growth of ZnO Films on Si(111), *J. Mater. Res.*, 2002, **17**, 2480–2483, DOI: 10.1557/JMR.2002.0361.
47 F. Khatkhatay, A. Chen, J. H. Lee, W. Zhang, H. Abdel-Raziq and H. Wang, Ferroelectric Properties of Vertically Aligned Nanostructured BaTiO3–CeO_2 Thin Films and Their Integration on Silicon, *ACS Appl. Mater. Interfaces*, 2013, **5**, 12541–12547, DOI: 10.1021/am403834k.
48 J. Huang, A. Gellatly, A. Kauffmann, X. Sun and H. Wang, Exchange Bias Effect along Vertical Interfaces in La0.7Sr0.3MnO3:NiO Vertically Aligned Nanocomposite Thin Films Integrated on Silicon Substrates, *Cryst. Growth Des.*, 2018, **18**, 4388–4394, DOI: 10.1021/acs.cgd.8b00366.
49 M. Buczek, M. Pohlmann, Z. Liu, Z. Moos, A. Gutsche, P. Cao, J. Mayer, W. Stein and R. Dittmann, Large Area

Pulsed Laser Deposition of Memristive Pr0.7Ca0.3MnO3 Heterostructures for Neuromorphic Computing, *Thin Solid Films*, 2024, **805**, 140499, DOI: 10.1016/j.tsf.2024.140499.

50 Z. Vakulov, D. Khakhulin, E. Zamburg, A. Mikhaylichenko, V. A. Smirnov, R. Tominov, V. S. Klimin and O. A. Ageev, Towards Scalable Large-Area Pulsed Laser Deposition, *Materials*, 2021, **14**, 4854, DOI: 10.3390/ma14174854.

51 Inc, P.P. PLD Production Systems - PVD Products Available online: https://www.pvdproducts.com/pulsed-laser-deposition-systems/pld-production-systems (accessed on 9 September 2025).

52 Y. Zhao, Y. Wu, A. Goyal, H. Huhtinen, P. Paturi and Y. Tsuchiya, Commercial Compact Fusion Triggered REBCO Tape Industry: Pulsed Laser Deposition Technology Opportunities and Challenges, *Superconductivity*, 2025, **15**, 100188, DOI: 10.1016/j.supcon.2025.100188.

53 P. Varade, A. H. Pandey, R. Selvamani, N. Venkataramani and A. R. Kulkarni, Tuning Structural, Dielectric, and Ferroelectric Properties of BTO-Based Ceramics through Dual-Site Substitution, *Mater. Chem. Phys.*, 2024, **319**, 129381, DOI: 10.1016/j.matchemphys.2024.129381.

54 C.-H. Hong, H.-P. Kim, B.-Y. Choi, H.-S. Han, J. S. Son, C. W. Ahn and W. Jo, Lead-Free Piezoceramics – Where to Move On?, *J. Materiomics*, 2016, **2**, 1–24, DOI: 10.1016/j.jmat.2015.12.002.

55 S. H. Park, J. Y. Kim, J. Y. Song and H. W. Jang, Overcoming Size Effects in Ferroelectric Thin Films, *Adv. Phys. Res.*, 2023, **2**, 2200096, DOI: 10.1002/apxr.202200096.